CryoTEMPO-EOLIS

Elevation Over Land Ice from Swath

Algorithm Theoretical Basis Document

Land Ice Elevation Thematic Point Product

Land Ice Elevation Thematic Gridded Product

Issue: 2.1

Date: 15th March 2023

Approval

Name	Date	Signed
Jerome Bouffard ESA		
Noel Gourmelen University of Edinburgh	23rd March 2023	
Martin Ewart Earthwave	23rd March 2023	

Document Versions

Issue	Date	Author	Reason for change
1.0	8th Nov 2021	Carolyn Michael	First version of document
1.1	29th Dec 2021	Martin Ewart	Updated and reviewed
2.0	5th Sept 2022	Livia Jakob, Carolyn Michael, Sophie Dubber	Updated for CryoTEMPO EOLIS Baseline 2
2.1	15th March 2023	Livia Jakob, Carolyn Michael, Sophie Dubber	Updated for release of CryoTEMPO-EOLIS Baseline 2

Table of Contents

List of acronyms

DEM	Digital Elevation Model
EO	Earth Observation
EOLIS	Elevation Over Land Ice from Swath
ESA	European Space Agency
FTP	File Transfer Protocol
GDAL	Geospatial Data Abstraction Library
GS	Ground Segment
LRM	Low Resolution Mode
NetCDF	Network Common Data Form (binary file format)
OIB	Operation Ice Bridge
PDGS	Payload Download Ground Segment
POCA	Point-Of-Closest-Approach
SARIn	Synthetic Aperture Radar Interferometric
STSE	Support To Science Element
UoE	University of Edinburgh
UTC	Coordinated Universal Time
XML	Extensible Mark-up Language

1. Introduction

1.1 Purpose and Scope

This document contains the Algorithm Theoretical Basis for the ESA CryoTEMPO-EOLIS project. The ATBD describes the scientific background and principle of the algorithms, their expected or known accuracy and performance, the input and output data, as well as capabilities and limitations. The CryoTEMPO-EOLIS consists of two distinct products;

1) a point product containing elevation point measurements with an associated uncertainty
2) a gridded product containing a spatial interpolation of the point product onto a uniform grid of elevations and corresponding uncertainty

This product covers three main regions: Antarctic ice sheet, Greenland ice sheet and the glacier regions, as defined by IMBIE (The IMBIE Team, 2018; The IMBIE Team, 2020) and RGI 7.0 (RGI Consortium, 2017). The glacier regions include Iceland, Svalbard, Arctic Canada, Russian Arctic, Alaska, Southern Andes, High Mountain Asia, the peripheral glaciers in Antarctica and the peripheral glaciers in Greenland.

1.2 Reference Websites

CryoTEMPO-EOLIS Project Website: http://cryotempo-eolis.org/

CryoTOP Evolution: https://cryotop-evolution.org/

CryoSat + Mountain Glaciers: http://www.cryosat-mtg.org/

ESA CryoSat-2 Data Download: https://science-pds.cryosat.esa.int/

Operation IceBridge: https://nsidc.org/data/icebridge/

Arctic DEM: https://www.pgc.umn.edu/data/arcticdem/

REMA DEM: https://www.pgc.umn.edu/data/rema/

Gapless-REMA100: https://figshare.com/articles/dataset/Gapless-REMA100/19122212

SRTM DEM: https://srtm.csi.cgiar.org/

ICESat-2: https://icesat-2.gsfc.nasa.gov/

Randolph Glacier Inventory (RGI) 7.0: https://glims-rgi.github.io/rgi_user_guide/welcome.html

2. Scientific Background

Global ice loss has been increasing over the past decades, with large contributions from glaciers, as well as from the two ice sheets (Slater et al., 2021). Global and continuous monitoring of these environments however remains a challenging task with estimates relying on a variety of observations and models to achieve the required spatial and temporal coverage.

CryoSat-2 is the first altimeter to carry a SAR interferometer, which allows a sharper footprint and the ability to precisely locate the position of the ground echo (Wingham et al., 2004). In practice, CryoSat's revolutionary interferometric design has allowed several technical breakthroughs and led to the application of radar altimetry to environments that were previously unforeseen. The conventional method of processing CryoSat-2 waveforms measures surface elevations at the Point-Of-Closest-Approach (POCA), sampling one elevation measurement per waveform at the closest point on the Earth's surface beneath the satellite. In contrast, the novel swath processing technique extracts multiple elevation measurements across the waveform, increasing the data volume and improving spatial as well as temporal coverage, enabling the use of CryoSat-2 measurements in new environments such as on mountain glaciers (Gourmelen et al., 2018).

Following on from the early demonstration of the technique and its potential impact, the "CryoSat ThEMatic PrOducts – SWATH Cryo-TEMPO" project (CryoTEMPO-EOLIS) consolidates the research and development undertaken during the CryoSat+ CryoTop / CryoTop evolution ESA STSE projects (Gourmelen et al., 2018) and the CryoSat+ Mountain Glaciers project (Jakob et al., 2021; Foresta et al., 2018; Foresta et al., 2016) into operational products. The purpose of the thematic products is to make the data available to the wider scientific community in a form that does not require a detailed understanding of the sensor used and extensive processing. This product allows users to perform analysis using swath data, and provides an uncertainty metric on which to filter the data to a desired precision.

3. Processing

The processing chain to generate the thematic products consists of multiple phases. The diagram below illustrates the sequence of steps in the processing chain.

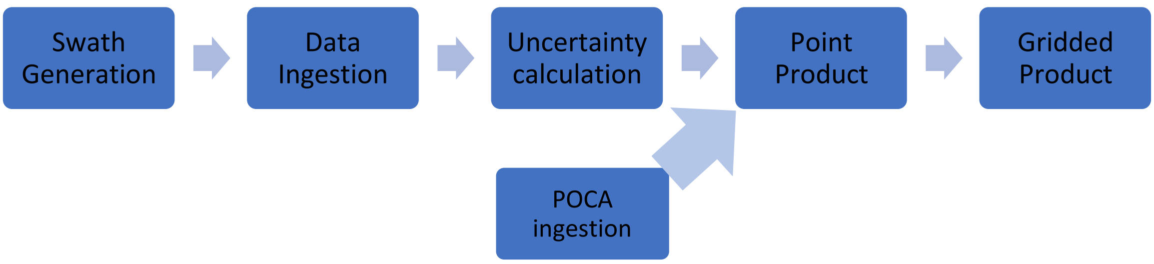

Figure 1: Processing Chain Sequence.

The swath generation as described in (Gourmelen et al., 2018) uses the along track L1B files and a reference DEM to compute a set of points perpendicular to the satellite's track referred to as the swath points. The data ingestion phase builds a spatial and temporal index of the along track data into 100 x 100 km tiles. The uncertainty value for a given point of data is computed using these tiles.

The Level 2 Baseline D NetCDF feed is used to source the POCA data that is ingested and used to create the point and gridded products. The columns used are: *height_1_20_ku* for the elevations, *retracker_1_quality_20_ku* for retracker quality filtering, *lat_poca_20_ku* and *lon_poca_20_ku* for position. The ESA CryoSat Product Handbook contains definitions of the column names (ESA, 2019).

The latitude and longitude coordinates are transformed to a local coordinate system using a consistent projection with the swath point data (see Table 1). The difference of POCA elevation to the reference DEM is used as a filter for erroneous data excluding any POCA points that are greater than 100m in difference from a reference DEM. The POCA data is also filtered on *retracker_1_quality_20_ku,* excluding points with a retracker quality metric equal to 0. These points are excluded because they correspond to locations where the retracker has failed, and the point position that has been recorded has defaulted to nadir.

3.1 Coordinate System and Geographic Projection

The latitude and longitude scales have distortion at the poles, which is a particular issue for the regions of interest in the CryoTEMPO-EOLIS operational products. Polar Stereographic coordinates have been chosen for the Greenland and Antarctica products, as these are commonly used in the community. For the glacier regions, those within the polar regions also use Polar Stereographic coordinates. Areas outside the polar regions are projected in latitude and longitude. Polar coordinates are consistent in terms of area and can be used in distance calculations. Projections for each of the EOLIS product regions are detailed in Table 1.

Table 1: Regional projections for EOLIS products.

Region	EPSG Code	Proj4 Code
Greenland Ice sheet/Periphery	3413	"+proj=stere +lat_0=90 +lat_ts=70 +lon_0=-45 +k=1 +x_0=0 +y_0=0 +datum=WGS84 +units=m +no_defs"
Antarctica Ice sheet/Periphery	3031	"proj4":"+proj=stere +lat_0=-90 +lat_ts=-71 +lon_0=0 +k=1 +x_0=0 +y_0=0 +datum=WGS84 +units=m +no_defs"
Iceland	3413	"+proj=stere +lat_0=90 +lat_ts=70 +lon_0=-45 +k=1 +x_0=0 +y_0=0 +datum=WGS84 +units=m +no_defs"
Svalbard	3413	"+proj=stere +lat_0=90 +lat_ts=70 +lon_0=-45 +k=1 +x_0=0 +y_0=0 +datum=WGS84 +units=m +no_defs"
Arctic Canada North/South	3413	"+proj=stere +lat_0=90 +lat_ts=70 +lon_0=-45 +k=1 +x_0=0 +y_0=0 +datum=WGS84 +units=m +no_defs"
Alaska	3413	"+proj=stere +lat_0=90 +lat_ts=70 +lon_0=-45 +k=1 +x_0=0 +y_0=0 +datum=WGS84 +units=m +no_defs"
Russian Arctic	3413	"+proj=stere +lat_0=90 +lat_ts=70 +lon_0=-45 +k=1 +x_0=0 +y_0=0 +datum=WGS84 +units=m +no_defs"
Southern Andes	4326	"+proj=longlat +ellps=WGS84 +datum=WGS84 +no_defs"
Central/South East/South West Asia	4326	"+proj=longlat +ellps=WGS84 +datum=WGS84 +no_defs"

4. Point Product

The CryoTEMPO-EOLIS point product is a set of high quality CryoSat-2 swath altimetry point data with uncertainty metrics applied. This product is designed to be user-friendly, so that it can be used by non-altimetry experts. The point products cover the following regions: Antarctic and Greenland ice sheets and peripheral glaciers, as well as the ice caps and glaciers in Iceland, Svalbard, Alaska, Arctic Canada, Russian Arctic, Southern Andes and High Mountain Asia. The definition of these regions follows the IMBIE definition of the Greenland and Antarctic Ice sheet, and the RGI7 definition of the glacier area.

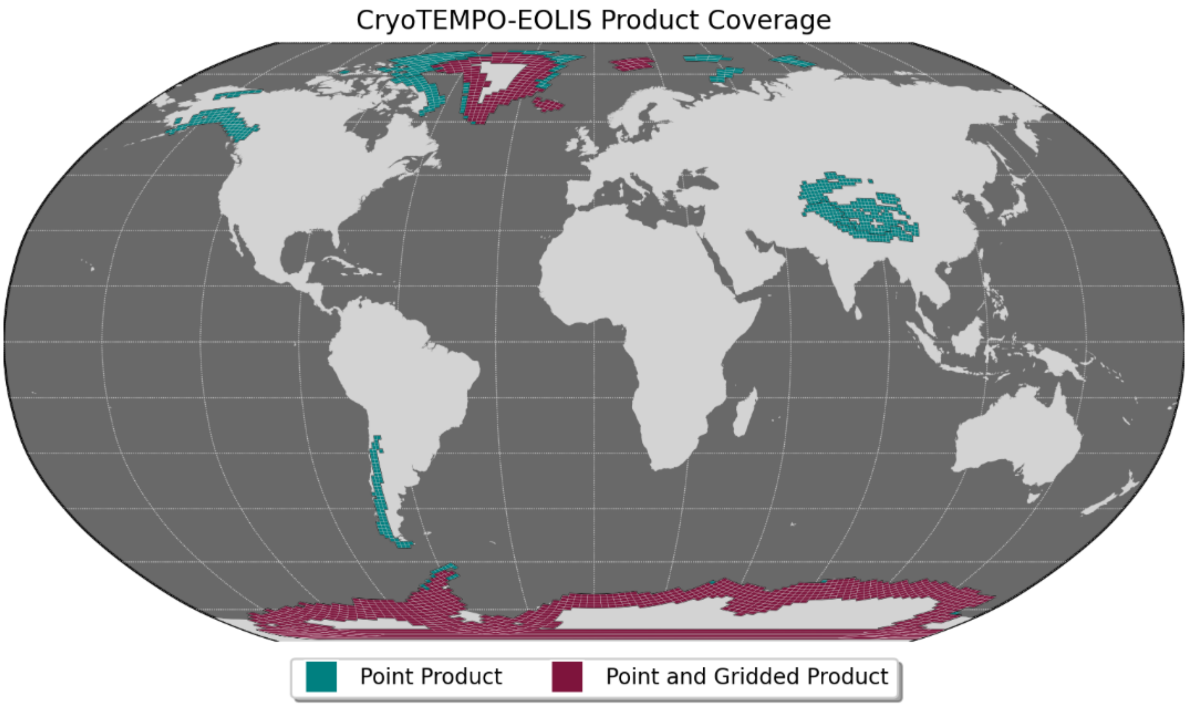

Figure 2: CryoTEMPO-EOLIS point product coverage illustrated using grid cells of 100km resolution.

4.1 Point Product Algorithm Description

4.1.1 Swath Processing

Swath processing of CryoSat-2 data has been detailed as part of the CryoSat+ CryoTop / CryoTop evolution ESA STSE projects (Gourmelen et al., 2018).

4.1.2 Phase Model Adjustment

Due to CryoSat-2's slight mis-pointing, the conversion from interferometric phase to angle of arrival is complex and leads to systematic errors in the angle of arrival (Wingham et al., 2004; Recchia et al., 2017). These errors are a function of surface slope, roll angle and distance from POCA. This affects predominantly areas of low surface slopes and leads to artefacts in the EOLIS elevation products (Figure 3). We mitigate this effect using a simple empirical model applied on a waveform basis to the elevation difference between swath and a reference DEM, taking advantage of the systematic nature of the error. For this, the swath waveforms are split into two sections: the *leading edge*, and *non-leading edge*. The *leading-edge* section begins at the POCA and continues until the return signal power peaks. The *non-leading edge* begins at the trailing edge until the end of the swath waveform. A robust linear model is fit to the data within the *leading-edge* section, and a two-part piecewise linear model fit to data within the *non-leading edge*. The model is then applied to the original swath data, ensuring that the mean elevation difference between swath and the reference model is maintained. Underlying topography is considered when applying the adjustment such that only very flat areas with low slope are adjusted. The degree of improvement of the model is also measured to determine if the adjustment should be applied. This approach works well to greatly reduced features present in the product, with only minor residuals remaining (Figure 3).

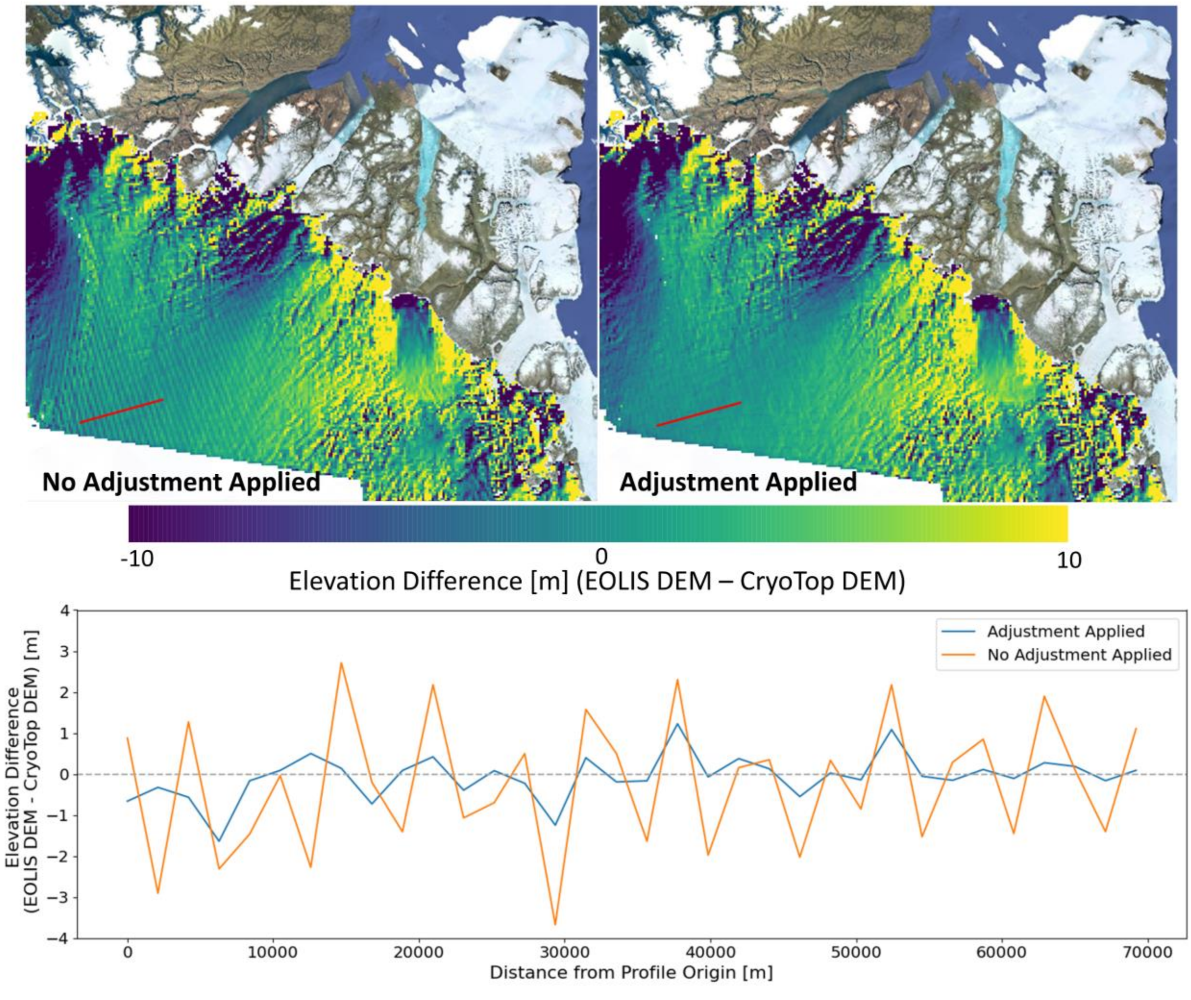

Figure 3: Example of improvement of phase model features in north Greenland. Top: elevation difference between the CryoTEMPO-EOLIS Greenland ice sheet gridded product for February 2019 and the CryoTop Greenland gridded DEM (Gourmelen et al., 2018) before (left) and after (right) the adjustment is applied. Bottom: elevation difference profile over the red line marked in the spatial plot (top), showing the reduction in amplitude of features after the adjustment is applied.

4.1.3 Point Product Uncertainty Score

For each swath elevation measurement an uncertainty value is calculated using a binning approach with several variables associated with measurement quality. This provides a simple metric on which the data can be filtered to a desired precision. This section outlines the elevation uncertainty algorithm.

Firstly, for each region, the swath data is compared to a reference elevation dataset (see Section 4.2.3 for details):

$$\Delta E = E_{swath} - E_{ref}$$

where E_{swath} and E_{ref} are the swath and reference elevations respectively joined within a 10-day time window and 50m radius. A slope correction is applied to ΔE to minimise errors due to variation in topography within the 50m joined distance. The differences, ΔE, are made up of errors in swath dataset, errors in the reference dataset, signal penetration differences between $E_{swath}$and E_{ref}, errors due to variation in elevation within the 10-days period, errors in the slope correction of the 50m joined criteria, as well as other systematic differences. Consequently, it cannot directly be used as a measure of data uncertainty.

A binning approach is then used to calculate standard deviations of the elevation differences ΔE using bins of six different variables, known to impact swath uncertainty (Table 2).

Table 2: Swath point data variables used for elevation uncertainty calibration.

Power in Decibels	As defined in the CryoSat-2 Product Handbook (ESA, 2019)
Coherence	As defined in the CryoSat-2 Product Handbook (ESA, 2019)
Distance to POCA	Distance in metres between the Swath observation and the POCA derived using the TFRMA retracker (Helm et al., 2014)
Along Track Slope	Slope is calculated along the track at a length scale of 400m (the along track resolution stated in ESA CryoSat-2 Product Handbook (ESA, 2019)). Along track slope is defined as change in elevation in metres between 200m in front and 200m behind the observation divided by 400m.
Across Track Slope	Slope is calculated across the track at a length scale of 1600m (the across track pulse limited footprint stated in ESA CryoSat-2 Product Handbook (ESA, 2019)). Across track slope is defined as change in elevation in metres between 800m to the left and 800m to the right of the observation divided by 1600m.
Roughness	Calculated from the reference DEM using the GDAL library function “gdaldem roughness”.

A six-dimensional cube consisting of each variable binned into 6 equal volume bins is generated. The data is sampled using every bin combination across all variables resulting in 6^6 (= 46,656) "quality bins". The quality bins are calculated separately for Antarctic Ice Sheet, Greenland Ice Sheet, and all Glacier regions apart from High Mountain Asia. For High Mountain Asia, the *Distance to POCA* variable was removed as sample data size for the uncertainty calculation was not sufficiently large enough.

The standard deviation is calculated from the binned sampled data which gives a range of high to low quality combinations of variables. To ensure that the sample size in each bin is considered, the upper bound of the confidence interval of the standard deviation is calculated:

$$\sigma \leq s\sqrt{\frac{n-1}{\chi^2_{1-\alpha/2}}}$$

where s is standard deviation of the sample, n is sample size, χ^2 is the Chi-square distribution and α is set to 0.05 to give a one-sided 97.5% confidence interval. This upper estimate of the standard deviation is defined as the uncertainty value for each of the quality bin combinations.

The quality bins are then used as a lookup table, where each individual swath elevation measurement is matched to an uncertainty, given its six variable values (see Table 2). It should be noted that the uncertainty metric provided is not a guarantee that the elevation is accurate to within the uncertainty score given. Moreover, it means that for the test sample data, there is a 97.5% confidence that the true standard deviation of the data will be less than the uncertainty score for a combination of variables. In other words, it is a conservative estimate of the uncertainty for a point but does not guarantee the point is not an outlier.

4.2 Point Product Input Data

4.2.1 Input Swath Elevation Data

Before the uncertainty score is calculated, the following baseline filters are applied to the swath elevation data to remove any weak signal and poor-quality data:

- Power in Decibels > -160 dB (Antarctic and Greenland ice sheets, Glacier regions, excluding High Mountain Asia), >-175 dB (High Mountain Asia)
- Power Scaled > 100
- Coherence > 0.6
- Absolute difference to a reference DEM <100 m
- Median absolute deviation of swath compared to reference DEM < 6m (Antarctic and Greenland ice sheets), <10m (glacier regions)

These filters were based on standard filter criteria used in the CryoSat+ CryoTop / CryoTop evolution ESA STSE projects (Gourmelen et al., 2018) and then adapted based on comparisons to reference datasets (such as OIB (Studinger, 2014) and ICESat2 (Smith et al., 2021)) to find values which minimised the standard deviations of the elevation difference whilst also maintaining an optimal volume of points. The minimum power in decibels threshold was lowered over High Mountain Asia to reflect the mean power of the distribution due to high surface slope. For all glacier regions, the median absolute deviation of elevation difference was on average observed to be higher, due to the more complex topography, compared to Greenland and Antarctic ice sheets and as a result the threshold was raised to 10 m.

4.2.2 Reference DEMs

Different reference DEMs across the regions. The Arctic DEM mosaic is used for Greenland, Iceland, Svalbard, Russian Arctic, Arctic Canada and Alaska (Porter et al., 2018), the Gapless-REMA100 DEM is used for Antarctica (Dong et al., 2022), and TanDEM-X DEM is used for Southern Andes and High Mountain Asia (German Aerospace Center (DLR), 2018). Pixels with no TanDEM-X values are filled with the SRTM DEM (Jarvis et al., 2008).

4.2.3 Uncertainty Calibration Data Sets

ATL06 (ATLAS/ICESat-2 L3A Land Ice Height; Advanced Topographic Laser Altimeter System) data (Smith et al., 2021) is used as a reference data set for all EOLIS regions.

For the High Mountain Asia quality bins, a combination of all joined data over High Mountain Asia and Alaska is used which is roughly an equal split across both regions. The Alaska data was used to increase data volume for the uncertainty calculation.

4.3 Point Product Uncertainty Score Output

The algorithm provides a six-dimensional cube consisting of the six variables binned into six equal volume bins with associated 97.5% upper one-sided confidence bound for each combination (Table 3). For each swath point, the associated variables are matched to the bin definitions and the estimated uncertainty score for that bin is assigned to the swath point.

Table 3: Definition of uncertainty bins for Antarctic ice sheet, Greenland ice sheet, glacier regions and High Mountain Asia. Each bin is between two bin edges, e.g. 0-1, 1-2 …. 5-6.

Antarctica

Bin Edge	Power [dB]	Coherence	Roughness	Slope Across	Slope Along	Distance To POCA [m]
0	-160.00	0.600	0.00	-0.3612	-0.4640	0
1	-157.23	0.773	0.87	-0.0105	-0.0070	4130
2	-154.80	0.852	1.43	-0.0050	-0.0024	6413
3	-152.49	0.900	2.17	-0.0020	0.0001	7793
4	-150.04	0.933	3.33	0.0000	0.0027	9314
5	-146.76	0.957	5.43	0.0042	0.0074	11126
6	0.00	1.010	128.20	0.3624	0.2626	22544

Greenland

Bin Edge	Power [dB]	Coherence	Roughness	Slope Across	Slope Along	Distance To POCA [m]
0	-160.00	0.600	0.00	-0.3492	-0.6794	0
1	-157.09	0.813	1.01	-0.0123	-0.0078	3649
2	-154.52	0.885	1.73	-0.0066	-0.0026	6104
3	-151.98	0.921	2.62	-0.0034	0.0000	7703
4	-149.22	0.946	3.85	-0.0008	0.0028	9387
5	-145.67	0.965	5.93	0.0074	0.0077	11255
6	0.00	1.000	239.80	0.4041	0.5017	22894

Glacier Regions

Bin Edge	Power [dB]	Coherence	Roughness	Slope Across	Slope Along	Distance to POCA [m]
0	-160.00	0.600	0.00	-0.5013	-0.8264	0
1	-158.14	0.802	3.91	-0.0239	-0.0226	366
2	-156.19	0.881	5.46	-0.0124	-0.0097	1421
3	-154.13	0.923	6.98	-0.0016	0.0002	3103
4	-151.84	0.949	8.87	0.0114	0.0106	5108
5	-148.78	0.969	11.89	0.0240	0.0235	7364
6	0.00	1.000	299.18	0.4724	0.8077	26944

High Mountain Asia

Bin Edge	Power [dB]	Coherence	Roughness	Slope Across	Slope Along
0	-175.00	0.600	0.00	-0.5340	-1.0270
1	-167.70	0.719	6.04	-0.0397	-0.0408
2	-164.91	0.816	10.39	-0.0090	-0.0071
3	-161.74	0.891	16.78	0.0121	0.0144
4	-157.12	0.946	29.90	0.0434	0.0516
5	0.00	1.000	639.62	0.5360	0.9060

4.4 Choice of Uncertainty Score Variables

For each variable used in the uncertainty calculation (see Table 2) there is a clear link between the value of the variable and the uncertainty score (Figure 4).

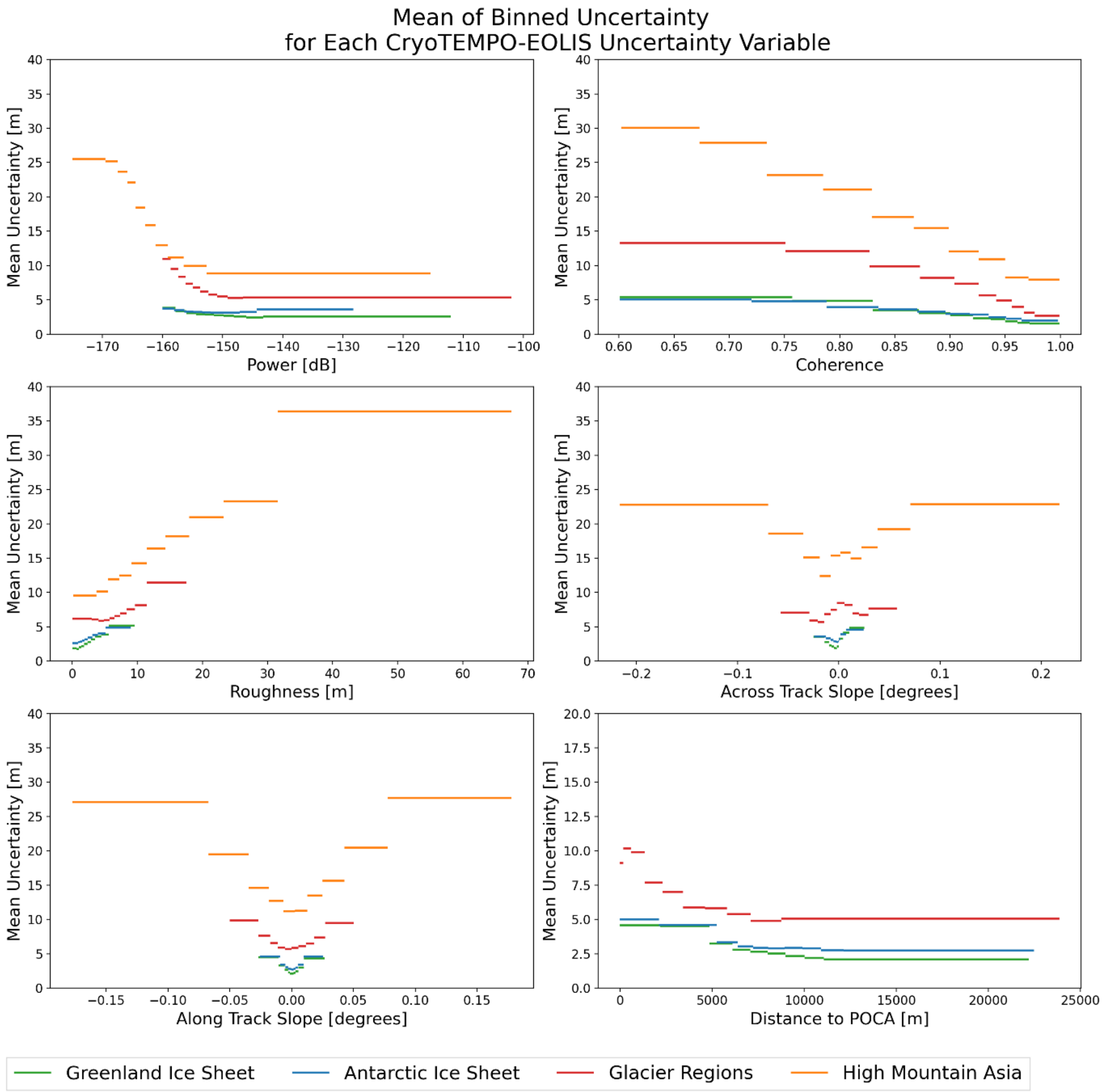

Figure 4: Comparison of uncertainty calculated using equal volume bins of points for each variable for glacier regions (red), High Mountain Asia (orange), Greenland ice sheet (green) and Antarctic ice sheet (blue). Uncertainty variables presented in this figure are defined in Table 2.

Note that Figure 4 illustrates the relationship between uncertainty and each individual variable as a comparison exercise, however the uncertainty calculation is a combination of all variables and thus is a six-dimensional relationship. Higher slope of the underlying terrain results in a higher uncertainty score: this is observed for *Along Track Slope* and A*cross Track Slope*. Swath data with high power in decibels results in a lower uncertainty score, with the opposite applying for low power data points. Similar linear correlations are observed for coherence where high coherence data has a low uncertainty score and low coherence data has a higher uncertainty score. The same relationship is recorded for the distance to the nearest POCA point, with swath points further from the POCA having a low uncertainty score. Finally, we see that data with low roughness, a measure of the irregularity of the surface, has a low associated uncertainty score, and higher roughness results in higher uncertainties.

5. Gridded Product

The CryoTEMPO-EOLIS gridded products are monthly DEMs that provide users with instant access to gridded and averaged point data at 2km spatial resolution. The CryoTEMPO-EOLIS DEMs are a valuable tool to monitor changes in topography at monthly temporal resolution. These products cover the Antarctic and Greenland ice sheets, as well as Austfonna ice cap in Svalbard and Vatnajökull ice cap in Iceland.

5.1 Gridding Algorithm Description

The gridded products are generated on a monthly basis, using the CryoTEMPO-EOLIS point product data, with each monthly DEM using a 3-month overlapping temporal window which is centred on the middle of the publication month. The gridding method uses the methods proposed by Jakob et al. (2021) to handle complex topography in the glacier regions.

There are multiple phases in the construction of the gridded product from the point data, which are detailed below:

1) **Topography removal:** topography is removed from the gridding by subtracting the reference DEM from the swath elevation measurements at a point level (hereinafter referred to as *DEM difference*).
2) **Median calculation:** for each 2km posting, all *DEM difference* values within a 2km radius are combined using a median calculation to create a gridded *DEM difference*.
3) **Padding:** the grid is padded with no data values for pixels that have no values
4) **Reduction of boundary noise and artefacts:** a median filter is applied iteratively 2 times to the gridded *DEM difference* values.
5) **Masking of data:** a 2km raster mask is created with the CryoSat-2 low resolution mode (LRM) mask removed over Greenland and Antarctic ice sheets, containing the region of interest of the product.
6) **Topography retrieval:** the gridded *DEM difference* values are converted back to a DEM using the reference DEM.

5.2 Gridded Product Input Data

For both, Greenland and Antarctica, the gridded product uses swath data points that have a maximum uncertainty of 7m as a quality filter. For both, Vatnajökull and Austfonna, the gridded product uses swath data points that have a maximum uncertainty of 20m as a quality filter. This is consistent with the maximum uncertainty filters applied to the point products.

5.3 Gridded Product Uncertainty Score

5.3.1 Uncertainty Propagation and Spatial Auto-Correlation

The point uncertainty is propagated to a gridded uncertainty, taking spatial auto-correlation into account. An uncertainty estimate is provided for each pixel using the following equation:

$$\sigma_p = \sqrt{\sum_{i}^{n} \frac{1}{n^2} \sigma_i^2 + \sum_{i}^{n} \sum_{j(j \neq i)}^{n} \frac{1}{n^2} \rho_{ij} \sigma_i \sigma_j}$$

where:

σ_p = Uncertainty of a pixel

σ_i, σ_j = Uncertainty of individual points

ρ_{ij} = Spatial auto-correlation between 2 points

n = Number of points contributing to a pixel

This equation reduces to the standard error of the mean uncertainty if all points have 0 correlation. Conversely, if all points are 100% correlated, the uncertainty is the mean of the uncertainties, which is a maximum of 20m given the maximum uncertainty of a point is 20m.

A semi-variogram is used to determine the spatial auto-correlation ρ_{ij} based on the separation of the points. This semi-variogram is calculated using the Python SciKit Gstat library.

For each region a sample of 50,000 is used to derive semi-variograms with: a maximum lag of 5km, an even binning function, the *stable model* and the *Cressie estimator*. Using the sill as an estimate for the covariance and the derived semi-variance, the estimated spatial auto-correlation as a function of distance between points is then calculated as:

$$\rho_{dist} = \frac{Sill - SV_{dist}}{Sill}$$

where:

ρ_{dist} = spatial auto-correlation for a given distance

SV_{dist} = Semi-variance for a given distance

A third order polynomial is then fit to the ρ_{dist} values between 0 and 5km to give an equation that can be used to estimate the spatial auto-correlation.

$$\rho(x) = ax^3 + bx^2 + cx + d$$

where x is the distance between observations. The calculated coefficients are provided in Table 4.

Table 4: Spatial auto-correlation coefficients for the four gridded regions.

Region	a	b	c	d
Austfonna	-1.2841e-11	1.2537e-7	-0.0004	0.4828
Vatnajökull	-8.8571e-12	9.7460e-8	-0.0004	0.5916
Greenland	-1.5253e-11	1.5099e-7	-0.0005	0.5994
Antarctica	-1.4327e-11	1.3909e-7	-0.0004	0.4910

Figure 5 shows an example of the spatial autocorrelation as a function of distance, for the Vatnajökull ice cap. This figure shows that for the applicable distance of 4000 m, the auto-correlation is small, and has a maximum of 0.49 when the distance is 0 m. This is expected as two independent observations at the same location will not be identical due to other uncertainties within the signal.

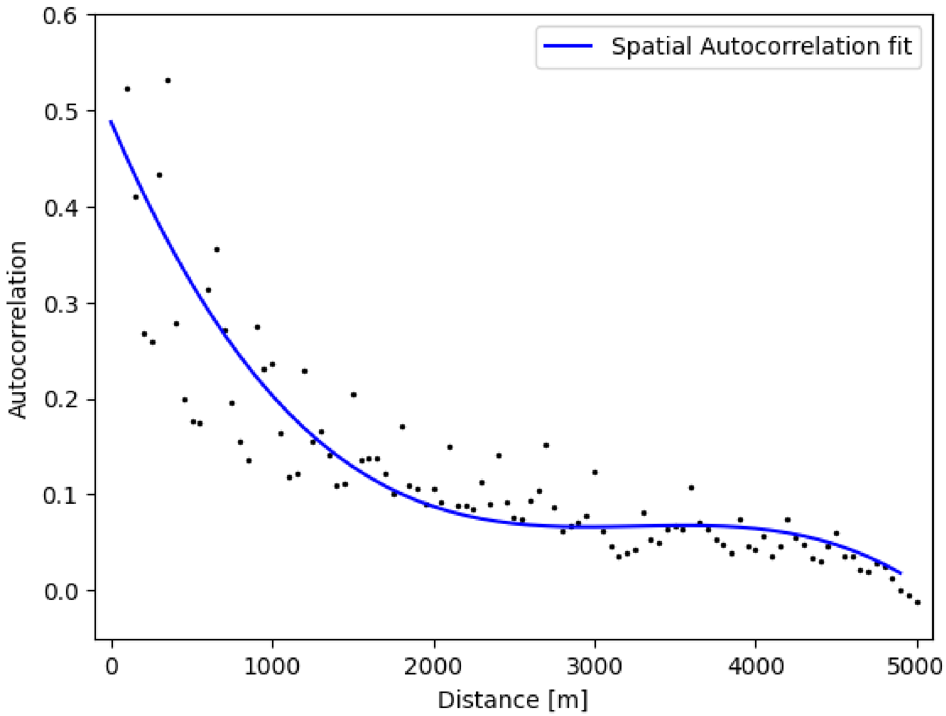

Figure 5: Spatial auto-correlation vs distance for the Vatnajökull ice cap.

Using the spatial auto-correlation, $\rho(x)$, the uncertainty formula shown previously means that in general, low pixel uncertainties of order 1-2 m are seen when there is a high volume of widely distributed points contributing to a pixel. Conversely much higher uncertainties are observed when there is a low volume of points or narrowly distributed points.

This can be demonstrated by looking at a pixel over time, as shown in Figure *6*. Outliers are clearly seen and highlighted by the uncertainty calculation.

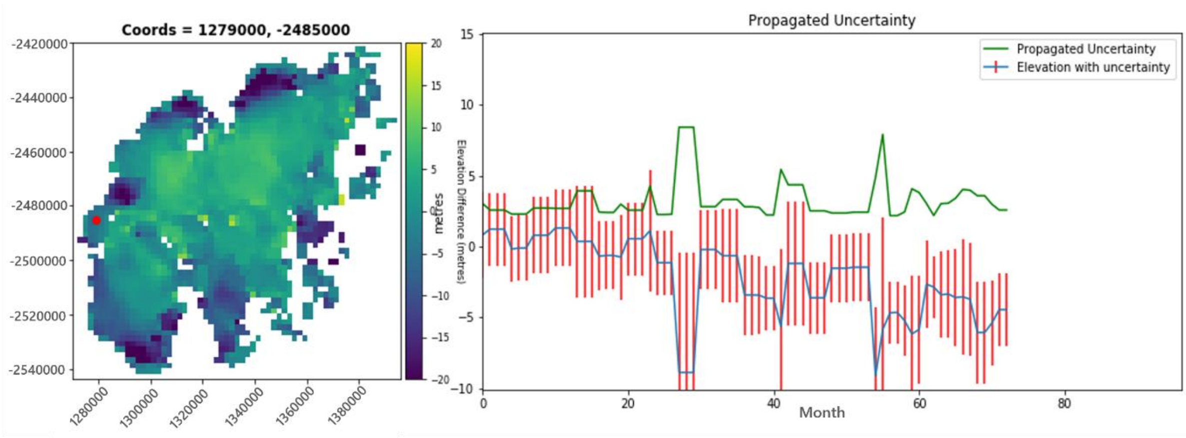

Figure 6: Example pixel near the edge of the Vatnajökull ice cap. Outlier values are showing a higher uncertainty.

5.3.2 Pre-Clustering

To improve computing performance the following intermediate step has been added to the calculation of the propagated gridded uncertainty for Greenland and Antarctica: all points within a distance of 100 m are pre-clustered and an effective uncertainty is calculated, assuming that they are all 100% spatially correlated. The reduced dataset is then propagated following the correlation model described in the previous section. This is motivated by the fact that points close to each other are indeed highly (>60%) correlated, and allows faster computation while maintaining a high level of accuracy.

6. References

Dong, Y., Zhao, J., Caiyong, L., & Liao, M. (2022). Gapless-REMA100: A gapless 100-m Reference Elevation Model of Antarctica with voids filled by multi-source DEMs. *ISPRS Journal of Photogrammetry and Remote Sensing*.

Dunse, T., Schellenberger, T., Hagen, J. O., Kääb, A., Schuler, T. V., & Reijmer, C. H. (2015). Glacier-surge mechanisms promoted by a hydro-thermodynamic feedback to summer melt. *The Cryosphere, 9*(1), 197-215. https://doi.org/10.5194/tc-9-197-2015

ESA. (2019). *CryoSat Baseline D Product Handbook.* https://earth.esa.int/documents/10174/125272/CryoSat-Baseline-D-Product-Handbook

Foresta, L., Gourmelen, N., Pálsson, F., Nienow, P., Björnsson, H., & Shepherd, A. (2016). Surface elevation change and mass balance of Icelandic ice caps derived from swath mode CryoSat-2 altimetry. *Geophysical Research Letters, 43*(12), 138-145. https://doi.org/10.1002/2016GL071485

Foresta, L., Gourmelen, N., Weissgerber, F., Nienow, P., Williams, J. J., Shepherd, A., Drinkwater, M. R., & Plummer, S. (2018). Heterogeneous and rapid ice loss over the Patagonian Ice Fields revealed by CryoSat-2 swath radar altimetry. *Remote Sensing of Environment, 211*, 441-455. https://doi.org/10.1016/j.rse.2018.03.041

German Aerospace Center (DLR). (2018). TanDEM-X - Digital Elevation Model (DEM) - Global, 90m. https://doi.org/10.15489/ju28hc7pui09

Gourmelen, N., Escorihuela, M. J., Shepherd, A., Foresta, L., Muir, A., Garcia-Mondéjar, A., Roca, M., Baker, S. G., & Drinkwater, M. R. (2018). CryoSat-2 swath interferometric altimetry for mapping ice elevation and elevation change. *Advances in Space Research, 62*(6), 1226-1242. https://doi.org/10.1016/j.asr.2017.11.014

Helm, V., Humbert, A., & Miller, H. (2014). Elevation and elevation change of Greenland. *Cryosphere, 8*(4), 1539-1559. https://doi.org/10.5194/tc-8-1539-2014

Hugonnet, R., McNabb, R., Berthier, E., Menounos, B., Nuth., C., Girod, L., Farinotti, D., Huss, M., Dussaillant, I., Brun, F., & Kääb, A. (2021). Accelerated global glacier mass loss in the early twenty-first century. *Nature, 592*, 726–731. https://doi.org/10.1038/s41586-021-03436-z

Jakob, L., Gourmelen, N., Ewart, M., & Plummer, S. (2021). Spatially and temporally resolved ice loss in High Mountain Asia and the Gulf of Alaska observed by CryoSat-2 swath altimetry between 2010 and 2019. *The Cryosphere, 15*(4), 1845-1862. https://doi.org/10.5194/tc-15-1845-2021

Jarvis, A., Reuter, H. I., Nelson, A., & Guevara, E. (2008). *'Hole-filled seamless SRTM data V4', International Centre for Tropical Agriculture (CIAT), available from https://srtm.csi.cgiar.org.*

McMillan, M., Shepherd, A., Gourmelen, N., Dehecq, A., Leeson, A., Leeson, A., Leeson, T., Leeson, A., Leeson, L., Benham, T., van den Broeke, M., Dowdeswell, J. A., Fettweis, X., Noël, B., & Strozzi, T. (2014). Rapid dynamic activation of a marine-based Arctic ice cap. *Geophysical Research Letters, 41*, 8902– 8909. https://doi.org/10.1002/2014GL062255

Porter, C., Morin, P., Howat, I., Noh, M.-J., Bates, B., Peterman, K., Keesey, S., Schlenk, M., Gardiner, J., Tomko, K., Willis, M., Kelleher, C., Cloutier, M., Husby, E., Foga, S., & Nakamura, H. (2018). ArcticDEM, Version 3. *Harvard Dataverse*. https://doi.org/10.7910/DVN/OHHUKH

Recchia, L., Scagliola, M., Giudici, D., & Kuschnerus, M. (2017). An Accurate Semianalytical Waveform Model for Mispointed SAR Interferometric Altimeters. *IEEE Geoscience and Remote Sensing Letter, 14*, 1537-1541.

RGI Consortium. (2017). Randolph Glacier Inventory - A Dataset of Global Glacier Outlines, Version 6. *NSIDC: National Snow and Ice Data Center*. https://doi.org/10.7265/4m1f-gd79

Rignot, E., Velicogna, I., van den Broeke, M. R., Monaghan, A., & Lenaerts, J. T. (2011). Acceleration of the contribution of the Greenland and Antarctic ice sheets to sea level rise. *Geophysical Research Letters, 38*. https://doi.org/10.1029/2011GL046583

Slater, T., Lawrence, I. R., Otosaka, I. N., Shepherd, A., Gourmelen, N., Jakob, L., Tepes, P., Gilbert, L., & Nienow, P. (2021). Review article: Earth's ice imbalance. *The Cryosphere*, 233–246.

Smith, B., Adusumulli, S., Csathó, B. M., Felikson, D., Fricker, H. A., Gardner, A., Holschuh, N., Lee, J., Nilsson, J., Paolo, F. S., Siegfried, M. R., Sutterley, T., & ICESAT-2 Science Team. (2021). ATLAS/ICESat-2 L3A Land Ice Height, Version 5. *NASA National Snow and Ice Data Center Distributed Active Archive Center*. https://doi.org/10.5067/ATLAS/ATL06.005

Studinger, M. (2014). IceBridge ATM L2 Icessn Elevation, Slope, and Roughness, Version 2. *NASA National Snow and Ice Data Center Distributed Active Archive Center*. https://doi.org/10.5067/CPRXXK3F39RV

The IMBIE Team. (2018). Mass balance of the Antarctic ice sheet from 1992 to 2017. *Nature, 558*(7709), 219-222. https://doi.org/10.1038/s41586-018-0179-y

The IMBIE Team. (2020). Mass balance of the Greenland Ice Sheet from 1992 to 2018. *Nature, 579*(7793), 233–239. https://doi.org/10.1038/s41586-019-1855-2

Wingham, D., Phalippou, L., Mavrocordatos, C., & Wallis, D. (2004). The mean echo and echo cross product from a beamforming interferometric altimeter and their application to elevation measuremen. *IEEE Transactions on Geoscience and Remote Sensing, 40*(10), 2305-2323. https://doi.org/10.1109/TGRS.2004.834352

Wouters, B., Gardner, A. S., & Moholdt, G. (2019). Global Glacier Mass Loss During the GRACE Satellite Mission (2002-2016). *Frontiers in Earth Science, 7*. https://doi.org/10.3389/feart.2019.00096